On the Extent of Longitudinal Finger Rotation in Publicly Available Finger Vein Data Sets

Bernhard Prommegger and Christof Kauba and Andreas Uhl
University of Salzburg
Jakob-Haringer-Str. 2
5020 Salzburg, AUSTRIA
{bprommeg, ckauba, uhl}@cs.sbg.ac.at

Abstract

Finger vein recognition deals with the identification of a subjects based on its venous pattern within the fingers. The majority of the publicly available finger vein data sets has been acquired with the help of scanner devices that capture a single finger from the palmar side using light transmission. Some of them are equipped with a contact surface or other structures to support in finger placement. However, these means are not able to prevent all possible types of finger misplacements, in particular longitudinal finger rotation can not be averted. It has been shown that this type of finger rotation results in a non-linear deformation of the vein structure, causing severe problems to finger vein recognition systems. So far it is not known if and to which extent this longitudinal finger rotation is present in publicly available finger vein data sets. This paper evaluates the presence of longitudinal finger rotation and its extent in four publicly available finger vein data sets and provides the estimated rotation angles to the scientific public. This additional information will increase the value of the evaluated data sets. To verify the correctness of the estimated rotation angles, we furthermore demonstrate that employing a simple rotation correction, using those rotation angles, improves the recognition performance.

1. Introduction

Biometric authentication systems have become well established nowadays. The most prominent examples are iris, face and fingerprint recognition systems. Recently, some emerging, new biometrics gain more attraction, especially hand and finger vein based systems as they provide several advantages over e.g. fingerprint based ones. Vein based systems utilize the patterns of the blood vessels inside the human body which are only visible in near infrared (NIR) light. This makes vein recognition systems more resistant against forgery. Moreover, the vein patterns are insensible to abrasion and skin surface conditions and a liveness detection can be performed easily [6]. The drawbacks of such systems compared to fingerprint based ones are the relatively large capturing devices and the low contrast and quality of the captured images. Furthermore, it is not clear if the blood vessel structure might be influenced by e.g. physical activity, temperature changes, certain injuries or diseases.

The performance of finger vein recognition systems is highly dependent on the quality of the acquired images. The acquisition quality is influenced by different internal and external factors, e.g. the quality of the illumination and camera module, ambient light or the presentation of the finger during acquisition. The later includes unintended finger movement during acquisition and finger misplacement in general. The influence of some kind of misplacements can be reduced by adding components to the scanner device, for example by adding a finger-shaped guiding surface to prevent a shift of the finger. However, finger tilt and longitudinal rotation of the finger are hard to avoid and pose severe problems for most finger vein recognition schemes. As finger vein systems evolve towards contact-less operation, problems due to finger misplacements will receive more attention in the future.

Performance degradations caused by various types of finger misplacement are not new and have been addressed in several publications. Kumar and Zhou [6] addressed the need for robust finger vein image normalization, including rotational alignment, already in 2012. Chen et al. [2] stated that deformations caused by a misplacement of the finger can be corrected either during pre-processing, feature extraction or comparison. Moreover, the design of the finger vein sensor helps to avoid or reduce misplacements of the finger as well. In [13] the authors showed, that longitudinal finger rotation has a severe influence on the recognition performance of a finger vein recognition system. There are several approaches that try to handle these issues during the

978-1-7281-3640-0/19/$31.00 ©2019 IEEE

processing of the vein patterns. Recognition schemes that claim to be resistant against finger misplacements to a certain extent are e.g. [7, 10, 15]. Huang et al. [3] improved the resistance against longitudinal rotation by applying an elliptical normalization to the input images. Chen et al. [2] tried to tackle the problem by detecting the deformation based on an analysis of the shape of the finger, e.g. around its longitudinal axis, and corrects the detected deformations using linear and non-linear transformations. However, none of theses approaches quantifies the extent (e.g. the rotation angle or the tilt angle) of the misplacement on which the deformation is based on. Besides these software based solutions, there are some hardware-based ones which aim to prevent finger misplacements during acquisition rather than correcting them. For example, Kauba et al. [5] presented a finger vein scanner that captures three fingers at once and requires the subject to place the fingers in an aligned position on a finger shaped guiding surface. This reduces longitudinal finger rotation, planar finger rotation as well as finger shifts to a minimum.

The main contribution of this work is the analysis of four public finger vein data sets on the presence of longitudinal finger rotation. Our analysis does not only indicate if longitudinal finger rotation is present, but also estimates the longitudinal rotation angle. This increases the value of those data sets for the scientific public as future evaluations on longitudinal finger rotation detection and correction can use the provided information as a reference. To verify our rotation detection results, we apply a simple rotation correction based on the estimated rotation angle and compare the recognition results of the original data set. The four finger vein data sets are UTFVP [14], SDUMLA-HMT [16], FV-USM [1] and PLUSVein-FV3 [4]. In contrast to the first three data sets, PLUSVein-FV3 should exhibit hardly any longitudinal finger rotation due to the design of the scanner device.

The rest of this paper is organized as follows: Section 2 describes longitudinal finger rotation and its impact on the recognition performance. Section 3 presents our proposed approach to detect and determine the longitudinal finger rotation present in a data set. Section 4 explains the processing tool-chain, the analysed data sets, the experimental set-up and discusses the results. Section 5 concludes this paper and gives an outlook on our future work.

2. Longitudinal Finger Rotation

Typically, finger vein scanners are designed to acquire only a single finger at a time. Different types of finger misplacement can easily occur with these scanners and pose a severe problem. Figure 1 shows the orientations of the x, y and z axis with respect to the finger. The different types of finger misplacement include planar shifts and rotation (shifts and rotations in the xy-plane) , shifts of the finger in z-direction (distance to the camera, scaling), finger bending, finger tilt (finger tip and root are not in the same xy-plane) and longitudinal finger rotation around the y-axis. As described in [13], the influence of some of these problematic misplacements can be reduced or even prevented completely during acquisition by adding simple support structures for finger positioning (e.g. guiding walls to prevent planar shifts) or corrected during pre-processing, feature extraction or comparison. Almost all currently available sensors are equipped with such support structures, but most of them still do not prevent a rotation around the y-axis (longitudinal finger rotation). Thus, longitudinal finger rotation cannot be ruled out and poses a severe problem to finger vein recognition systems.

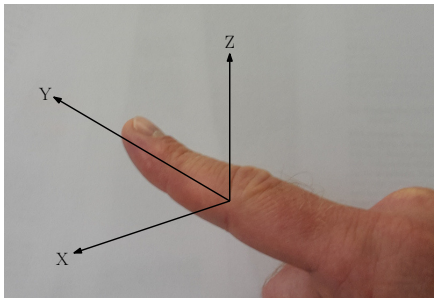

Figure 1. Definition of the axes of a finger in a three-dimensional space

The captured vein structure is a projection of the vessel structure in the 3D space onto a 2D plane. If the finger is rotated along its longitudinal axis, the vein pattern is deformed according to a non-linear transformation. Figure 2 shows the effect of longitudinal finger rotation on the vein pattern. The finger cross section (top row) is rotated from -30° to +30°. As a result of the rotation the projected pattern of the veins (bottom row) changes as well. Depending on the relative position of the veins to each other and the rotation angle, some of the captured veins might merge into a single one. The vein structures of -30° (left), 0° (middle) and 30° (right) are completely different. Widely used vein recognition schemes can handle such deformations only to a certain extent [13]. If the deformations caused by the longitudinal rotation are corrected, the negative effect can be reduced but not completely prevented.

3. Finger Rotation Detection

All publicly available finger vein data sets provide only images captured from one perspective. But a single image does not provide enough information to reliably calculate or estimate the longitudinal rotation angle. Therefore, we propose an empirical approach to estimate the rotation angle: All images in the data set are rotated in steps of 1° within the range of $\pm 45°$. Then the rotated images of a finger are

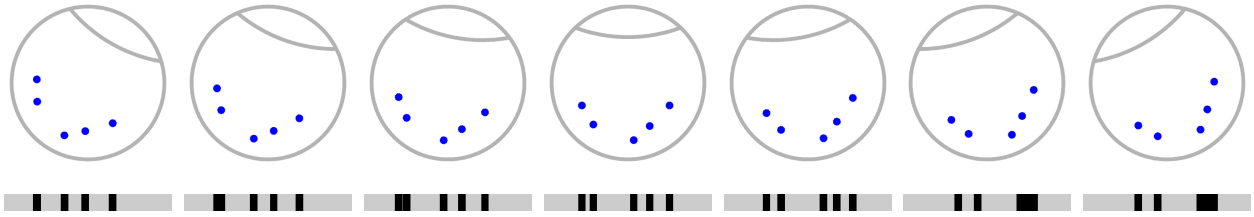

Figure 2. Longitudinal finger rotation principle: a schematic finger cross section showing five veins (blue dots) rotated from -30° (left) to +30° (right) in 10° steps. The projection (bottom row) of the vein pattern is different depending on the rotation angle according to a non-linear transformation (originally published in [13]).

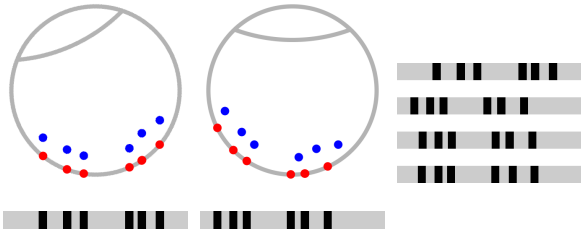

Figure 3. Principle of rotation correction. Left: finger rotated with 25°. The blue points depict the veins inside the finger, the cyan points the veins projected on the finger shape. The bar below is the projected vein pattern. Middle: the cyan points represent the rotation corrected vein pattern on the skin, the blue points represent the veins in the finger in its original position from the palmar view. The bar below is the rotation corrected vein pattern. On the right side the vein patterns are visualized below each other. From top to bottom: rotated vein pattern, corrected vein pattern, corrected pattern shifted for the highest correlation to the palmar pattern (bottom row).

compared to the first non rotated sample of this finger. The rotation angle is the angle, where the rotated an non rotated image shows the highest similarity, i.e. where the comparison score reaches its maximum. As more advanced vein recognition schemes, e.g. deformation tolerant feature point matching [10], try to compensate longitudinal rotation, they are not suitable for our approach. Thus, we opted to utilise Maxium Curvature (MC) [12], a simple vein pattern based feature extraction method and the comparison method proposed by Miura et al. in [11].

For an accurate correction of the vein pattern, in addition to the position of the veins in the 2D image, the shape of the finger and the depth of the veins within the finger must also be known. As this information is not available, both need to be estimated. We approximate the shape of the finger as a circle like Matsuda et al. did in [10]. We further assume, that the veins are located on the skin surface. Therefore, the vein pattern is projected back on the outer circle of the finger. Figure 3 depicts this principle. The left image shows a schematic cross section of a finger acquired under a longitudinal rotation of $\varphi_{rotate} = 25°$. The blue dots represent the veins in their proper position, the red ones those that are projected onto the skin. The bar below is a visualization of the vein pattern where the black areas correspond to the veins. In the middle image, the finger is rotated back into the ideal palmar position ($\varphi_{rotate} = 0°$). It is clearly visible, that the blue and red dots are not perfectly aligned with each other. The right side shows from top to bottom the vein patterns of the acquired image (same as on the left side), the rotated pattern (same as in the middle), a shifted version of the rotated pattern and the original pattern that would have been acquired without the presence of longitudinal rotation. It is clearly visible that the rotation corrected pattern is more similar to the original pattern than the acquired one. The additional shift is applied to achieve the highest possible correlation between the corrected and the original pattern.

The rotation of the veins by an angle of φ_{rotate} is calculated by applying a rotation matrix given in (1).

$$\begin{bmatrix} x_r \\ y_r \end{bmatrix} = \begin{bmatrix} cos(-\varphi_{rotate}) & -sin(-\varphi_{rotate}) \\ sin(-\varphi_{rotate}) & cos(-\varphi_{rotate}) \end{bmatrix} * \begin{bmatrix} x \\ y \end{bmatrix} \quad (1)$$

x and y are the coordinates of the vein pixel in the acquired image, x_r and y_r the ones in the rotated image. x is the position of the pixel in the vein pattern, y is calculated by (2)

$$y = \sqrt{r^2 - x^2} \quad (2)$$

where r is the approximated radius of the finger.

The rotation angle $\varphi_{i,j}$ between two samples of the same finger is calculated by (3). $score(i, j, \varphi_{rotate})$ is the score, obtained by applying the Miura matcher [11] on the extracted MC features, of the i^{th} sample rotated by φ_{rotate} and the non rotated j^{th} sample.

$$\varphi_{i,j} = \underset{-45° \leq \varphi_{rotate} \leq +45°}{\arg\max} score(i, j, \varphi_{rotate}) \quad (3)$$

To achieve a more robust result, the final rotation angle $\Phi_{i,1}$ is calculated as the average of $\varphi_{i,1}$ (the calculated angle of

the rotated i^{th} sample against the non rotated 1^{st} sample) and $\varphi_{1,i}$ (the calculated angle of the rotated 1^{st} sample against the non rotated i^{th} sample):

$$\Phi_{i,1} = \text{avg}\left(\varphi_{i,1}.\varphi_{1,i}\right) \tag{4}$$

4. Experiments

The rotation angle is estimated based on the approach described in Section 3. We used Maximum Curvature as feature extractor as it usually achieves accurate results in extracting the vein patterns. The rotation angle of the samples is always calculated with respect to the first sample of the respective finger. In order to confirm the obtained rotation angles, we evaluate the recognition performance of the original data sets as well as on the rotation corrected ones and compare the results. The rotation correction has been done in two different ways: with respect to the first sample of the respective finger and with respect to the mean of the determined rotation angles of each finger.

4.1. Data Sets

We evaluate the longitudinal finger rotation of four different publicly available finger vein data sets:

- **SDUMLA-HMT [16]** is a multimodal biometric database that contains samples for face, gait, iris, fingerprint and finger veins from 106 individuals. The finger vein subset contains six fingers (ring, middle and index finger from both hands) per subject, captured in one session taking six images of each finger.
- **UTFVP [14]** contains six fingers (ring, middle and index finger from both hands) from 60 volunteers in two sessions. At each session two samples per finger were captured.
- **FV-USM [1]** was acquired from 123 volunteers, four fingers each (left and right index and middle finger). The data was captured in two different sessions, capturing six samples per finger in each session.
- **PLUSVein-FV3 [4]** contains palmar and dorsal images of 360 fingers from 60 different subjects (ring, middle and index finger from both hands) captured in one session with five samples per finger using two different variants of the same sensor: One utilizing NIR laser modules for illumination, the other one using NIR LEDs. The sensor was built in a way that requires the subject to place the whole hand flat on the sensor. Therefore, the data set is expected contain little to no longitudinal rotation. We only evaluate the dorsal images acquired by the laser version of the sensor.

Table 1 contains an overview on the statistics of the data sets.

Name	Subjects	Finger	Samples	Images	View
SDUMLA-HMT	106	6	6	3816	palmar
UTFVP	60	6	4	1440	palmar
FV-USM	123	4	12	5904	palmar
PLUSVein-FV3	60	6	5	1800	dorsal

Table 1. Evaluated finger-vein data sets

Name	Genuine	Impostor	Total
SDUMLA-HMT	9540	200340	209880
UTFVP	2160	63720	65880
FV-USM	32472	120048	152520
PLUSVein-FV3	3600	63720	67320

Table 2. Number of comparisons for each data set

4.2. Recognition Tool-Chain

The finger vein recognition tool-chain consists of the following components:

1. For **finger region detection** and **finger alignment** we use an implementation that is based on [8].
2. The **ROI extraction** differs from [8]. We do not cut a defined rectangle within the finger, but similar to [3], normalize the finger to a fixed width.
3. To improve the visibility of the vein pattern we use **High Frequency Emphasis Filtering** (HFE) [18], **Circular Gabor Filter** (CGF) [17] and simple **CLAHE** (local histogram equalisation) [19] as **preprocessing**.
4. As **feature extraction** method we employ the well-established vein-pattern based **Maximum Curvature** method [12].
5. The **comparison** of the binary feature images is done using a correlation measure, calculated between the input images and in x- and y-direction shifted and rotated versions of the reference image as described in [11].

An implementation of the recognition tool-chain is available for download on our website[1].

4.3. Experimental Protocol

To quantify the performance, the EER, the FMR100 (the lowest FNMR for FMR $\leq 1\%$), the FMR1000 (the lowest FNMR for FMR $\leq 0{,}1\%$) as well as the ZeroFMR (the lowest FNMR for FMR = 0%) are used. We follow the test protocol of the FVC2004 [9]: For calculating the genuine scores, all possible genuine comparisons are performed. For calculating the impostor scores, only the first image of a finger is compared against the first image of all other fingers. The resulting numbers of comparisons for all data sets are listed in Table 2. To quantify the increase of the performance, the relative performance increase (RPI) is used, which

[1] http://wavelab.at/sources/Prommegger19c

is calculated as stated in (5):

$$RPI_{x,ref} = \frac{EER_{ref} - EER_x}{EER_x}, \quad (5)$$

EER_{ref} is the EER of the reference data set and EER_x the EER of the evaluated data set.

4.4. Results

Table 3 shows the detected longitudinal rotation angles with respect to the reference image (first sample of every finger) as a histogram distribution with 5° bins. As expected, the PLUSVein-FV3 data set exhibits little to no rotation. 98.4% of the fingers lay within 0-5° of rotation. There is no sample that is rotated more than 10° from its reference. The detected rotation on the UTFVP is small as well. 85% of the samples are within 5°, 99.1% within 10° of rotation. Only 0.9% of the images exceed a rotation of 10°. FV-USM exhibits a slightly higher degree of longitudinal rotation than UTFVP. 80% of the samples are within 5°, 95.3% are within 10° and 4.7% of the samples are rotated more than 10°. SDUMLA-HMT shows the largest deviations caused by longitudinal finger rotation. Only 56.4% of the images are rotated less than 5°, whereas 5.6% exceeds a rotation of more than 20°. The largest rotation detected is 44.5°.

Table 4 contains statistical data regarding the longitudinal rotation of the different data sets, i.e. the distance of the rotation angles with respect to the mean rotation angle of each finger and the maximum rotation distance between two samples of the same finger. PLUSVein-FV3 shows the smallest deviations. In average, there is a rotation of 1.37° between two samples. The maximum distance to the mean value is 8.6°, the maximum rotation between two samples is 12.5°. For UTFVP, the average distance to the mean rotation angle is 2.65°. The maximum rotation between two samples is 29.5°. The results for FV-USM are slightly worse than for UTFVP. Also Table 4 confirms that the level of longitudinal rotation present in the SDUMLA-HMT is high. On average, two samples are rotated 6.43° against each other. The maximum rotation angle between two samples is 77°, which is astonishingly high.

In order to ensure that the determined 77° did not occur due to an calculation error, we examined the respective sample images visually. The mentioned rotation was determined between sample #4 and #6 of the left ring finger of subject #96. Figure 4 shows the samples: on the left #1 as reference image, #4 in the middle and #6 on the right. The top row shows the original images as contained the data set. It is clearly visible that the three samples are rotated versions of the same finger. The second row shows the extracted ROIs and the third row shows the rotation corrected version of the ROI using the determined rotation anlge $\Phi_{i,1}$. Sample #4 (middle column) is corrected by 44.5° and sample #6 (left column) by -32.5°. One can easy see that the rotation corrected ROIs are better aligned with respect to longitudinal rotation.

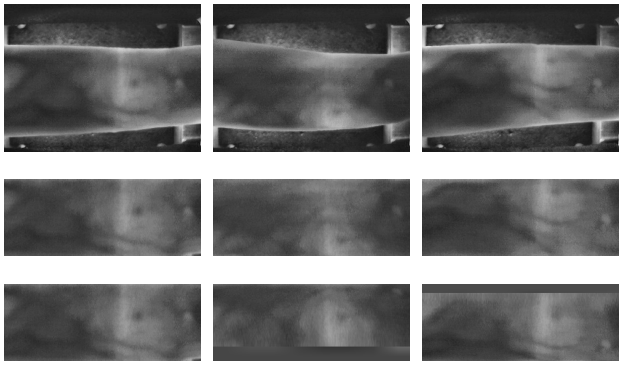

Figure 4. Three samples from the same finger (left ring finger of subject #96) of the SDUMLA-HTM data set. Top row: original images from data set, row 2: extracted ROI not rotated, row 3: corrected ROI. The left column shows sample #1 (reference image), the middle sample #4 (rotation angle: 44°) and the right sample #6 (rotation angle: -32°). All images are enhanced using CLAHE.

To verify the estimated rotation angles, the recognition performance for the original data sets (ORI) and the two corrected versions of the data sets have been evaluated: In the first version (ROT), all samples are corrected with respect to the first sample of each finger, in the second one (ROT Mean), all samples of a finger are corrected with respect to the calculated mean rotation angle of this finger. The rotation correction is done by applying the rotation matrix of Equation (1). The recognition performance results are given in Table 5. It also gives some statistics on the comparison score values, including the mean, minimum and maximum values for the genuine as well as for the impostor scores. The EER, FMR100, FMR1000 and ZeroFMR decreased for both correction scenarios. For SDUMLA-HMT, FV-USM and PLUSVein-FV3, the correction with respect to the first sample of a finger achieves the best result, for UTFVP the correction with respect to the mean rotation angle attains a superior performance. To point out the performance increase that can be gained by applying this simple rotation correction, the RPI as stated in Equation (5) is calculated too. For SDUMLA-HMT and UTFVP we arrive at a RPI of nearly 350%, for FV-USM of 120%. The lowest RPI is achieved for PLUSVein-FV3, which directly corresponds to the low level of longitudinal finger rotation present in this data set.

The improvement in terms of recognition performance is mainly due to a better separation of genuine and impostor scores. In Figure 5 the score distribution for the original SDUMLA-HMT data set (blue lines) and its corrected version (version 1, rotated to the first sample of a finger, red

Data Set	Rotation to mean								
	0° - 5°	5° - 10°	10° - 15°	15° - 20°	20° - 25°	25° - 30°	30° - 35°	35° - 40°	40° - 45°
SDUMLA-HMT	56.4%	21.5%	10.4%	6.2%	2.7%	1.6%	0.8%	0.4%	0.1%
UTFVP	85.2%	13.9%	0.8%	0.1%	-	-	-	-	-
FV-USM	80.0%	15.3%	3.7%	0.8%	0.2%	-	-	-	-
PLUSVein-FV3	98.4%	1.6%	-	-	-	-	-	-	-

Table 3. Distribution of longitudinal finger rotation in classes of size 5°.

Data Set	Absolute Distance to Mean			Maximum Distance		
	Mean	Max	Std	Mean	Max	Std
SDUMLA-HMT	6.43	44.83	6.90	19.40	77.00	15.73
UTFVP	2.65	16.50	2.29	7.95	29.50	4.41
FV-USM	3.04	23.83	3.23	11.32	41.00	7.75
PLUSVein-FV3	1.37	8.60	1.24	4.46	12.50	2.44

Table 4. Statistical data on the degree of rotation present in the data sets.

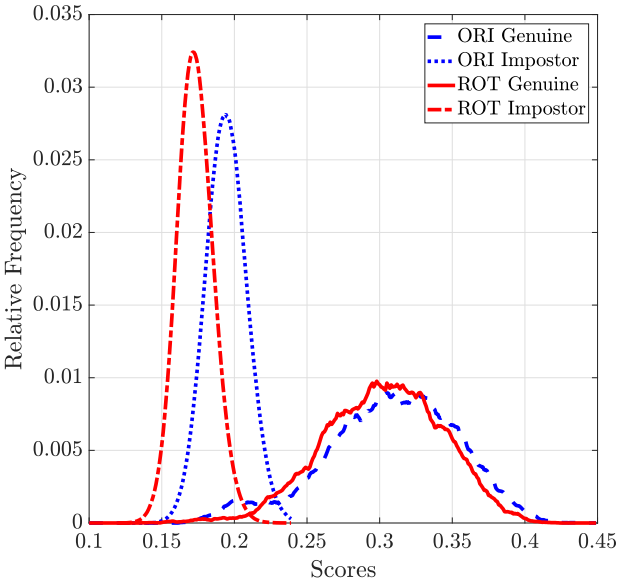

Figure 5. Distribution of genuine and impostor scores for SDUMLA-HMT: ORI = oiriginal data set, ROT = rotation corrected to 1st image

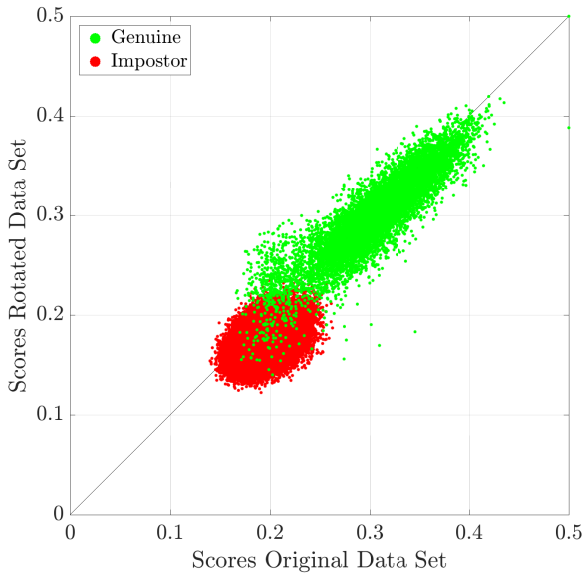

Figure 6. Changes in scores from the original data set to the rotation corrected data set

lines) is visualized. The impostor scores of the rotated images are lower in general compared to the scores obtained from the original data set. This is mainly due to the reduced extent of vertical shift that has to be applied during comparison for the corrected data set. In our set up, the shift range is reduced by a third compared to the value necessary to achieve the best results for the original data set. The reduction of the vertical shift also leads to a slight decrease in the genuine score values. However, this decrease is lower than for the impostor ones, which leads to a better separation of the scores in general. Moreover, the genuine scores of samples exhibiting a high degree of rotation are increased too (the accumulation of the original genuine scores around the score of 0.2 disappears after the correction). Figure 6 presents the shift in the score distributions in a different way by showing the change in their values. The score values of the original data set are plotted on the x axis while the ones of the corrected data set are plotted on the y axis. Due to the reduction of the individual impostor score values, the cluster corresponding to the impostor scores (red) moves slightly downwards. The genuine scores (green) move downwards too, but to a lower extent. The interesting part of the plot are those genuine scores that overlap with the impostor ones in the evaluation of the original data set. Most of these originally low genuine score are increased above the level of the impostor scores after the rotation correction. This becomes visible by the raise of the green genuine scores above the red impostor ones around the score of 0.2. Again, this visualises the better separation of genuine and impostor scores. The statistical values of the genuine and impostor scores in Table 5 confirm these visual observation.

Data Set	Version	Performance Indicators					Genuine Scores				Impostor Scores			
		EER	FMR100	FMR1000	ZeroFMR	RPI	Min	Mean	Max	Std	Min	Mean	Max	Std
SDUMLA-HMT	ORI	4.73 (±0.22)	6.12	8.09	63.25	-	0.17	0.31	0.44	0.05	0.14	0.19	0.33	0.01
	ROT	**1.07** (±0.11)	1.13	1.72	59.91	**341.6**	0.15	0.30	0.42	0.04	0.12	0.17	0.32	0.01
	ROT Mean	1.14 (±0.11)	1.18	1.82	47.77	315.8	0.14	0.30	0.42	0.04	0.12	0.17	0.30	0.01
UTFVP	ORI	0.42 (±0.12)	0.23	0.65	3.11	-	0.12	0.26	0.38	0.04	0.07	0.12	0.18	0.01
	ROT	0.19 (±0.09)	0.19	0.23	1.62	124.5	0.09	0.25	0.36	0.04	0.06	0.09	0.16	0.01
	ROT Mean	**0.09** (±0.06)	0.05	0.09	1.30	**349.1**	0.10	0.25	0.37	0.04	0.07	0.10	0.15	0.01
FV-USM	ORI	1.23 (±0.08)	1.30	2.34	5.27	-	0.13	0.25	0.36	0.03	0.11	0.15	0.19	0.01
	ROT	**0.56** (±0.05)	0.48	0.93	2.47	**120.1**	0.13	0.24	0.50	0.03	0.11	0.14	0.18	0.01
	ROT Mean	0.77 (±0.06)	0.69	1.42	3.93	59.4	0.13	0.24	0.40	0.03	0.11	0.14	0.19	0.01
PLUSVein-FV3	ORI	0.08 (±0.05)	0.03	0.08	0.39	-	0.08	0.20	0.32	0.04	0.05	0.07	0.09	0.00
	ROT	**0.06** (±0.04)	0.00	0.06	0.25	**50.0**	0.08	0.20	0.31	0.04	0.05	0.07	0.09	0.00
	ROT Mean	0.08 (±0.05)	0.00	0.08	0.22	0.9	0.08	0.20	0.32	0.04	0.05	0.07	0.09	0.00

Table 5. Recognition performance on the evaluated data sets and its corrected versions: ORI = original data set, ROT = rotation corrected to 1st image, ROT Mean = rotation corrected to mean of finger. Best achieved EER and RPI values are highlighted in bold.

5. Conclusion

It has been shown previously that longitudinal finger rotation poses a significant problem for many well-established recognition schemes [13]. This paper investigated on the presence and degree of longitudinal finger rotation in four publicly available finger vein data sets. The rotation angle between different samples of the same finger has been estimated based on an empirical approach using a correlation based comparison of the extracted vein patterns.

PLUSVein-FV3 showed the lowest degree of longitudinal finger rotation, followed by UTFVP and FV-USM, while SDUMLA-HMT exhibited the highest amount. The degree of longitudinal finger rotation present in the data set strongly depends on the design of the scanner device, the acquisition protocol and its supervision. In the PLUSVein-FV3 data set, the rotation is reduced to a minimum by requiring the subject to place the whole hand flat on the scanner device. The scanners used to acquire UTFVP, FV-USM, and SDUMLA-HMT were not built to avoid longitudinal finger rotation. Nevertheless, the small rotation present in UTFVP and FV-USM suggests that the acquisition protocol and supervision was very good.

Moreover, we applied a simple rotation correction and verified the determined rotation angles by comparing the recognition performance of the original data sets and their rotation corrected versions. It turned out that the recognition performance could be improved for all four data sets. The highest improvement could be achieved for SDUMLA-HMT and UTFVP with a performance increase of 350%. Even the correction of the low longitudinal rotation in PLUSVein-FV3 lead to a performance increase of 50%.

We provide the determined rotation angles for all four data sets in order to increase the value of those data sets by augmenting them with this additional information. These can be download at: `http://wavelab.at/sources/Prommegger19c`.

In our future work we will evaluate the presence of longitudinal finger rotation and its extent for further data sets as well as an inter-session analysis of data sets acquired in multiple sessions.

6. Acknowledgements

This project has received funding from the European Union's Horizon 2020 research and innovation program under grant agreement No. 700259.

References

[1] M. S. M. Asaari, S. A. Suandi, and B. A. Rosdi. Fusion of band limited phase only correlation and width centroid contour distance for finger based biometrics. *Expert Systems with Applications*, 41(7):3367–3382, 2014.

[2] Q. Chen, L. Yang, G. Yang, and Y. Yin. Geometric shape analysis based finger vein deformation detection and correction. *Neurocomputing*, 2018.

[3] B. Huang, Y. Dai, R. Li, D. Tang, and W. Li. Finger-vein authentication based on wide line detector and pattern normalization. In *Pattern Recognition (ICPR), 2010 20th International Conference on*, pages 1269–1272. IEEE, 2010.

[4] C. Kauba, B. Prommegger, and A. Uhl. Focussing the beam - a new laser illumination based data set providing insights to finger-vein recognition. In *Proceedings of the IEEE 9th International Conference on Biometrics: Theory, Applications, and Systems (BTAS2018)*, pages 1–9, Los Angeles, California, USA, 2018. accepted.

[5] C. Kauba, B. Prommegger, and A. Uhl. The two sides of the finger - dorsal or palmar - which one is better in finger-vein recognition? In *Proceedings of the International Conference of the Biometrics Special Interest Group (BIOSIG'18)*, Darmstadt, Germany, 2018.

[6] A. Kumar and Y. Zhou. Human identification using finger images. *Image Processing, IEEE Transactions on*, 21(4):2228–2244, 2012.

[7] E. C. Lee, H. C. Lee, and K. R. Park. Finger vein recognition using minutia-based alignment and local binary pattern-based feature extraction. *International Journal of Imaging Systems and Technology*, 19(3):179–186, 2009.

[8] Y. Lu, S. J. Xie, S. Yoon, J. Yang, and D. S. Park. Robust finger vein roi localization based on flexible segmentation. *Sensors*, 13(11):14339–14366, 2013.

[9] D. Maio, D. Maltoni, R. Cappelli, J. L. Wayman, and A. K. Jain. FVC2004: Third Fingerprint Verification Competition. In *ICBA*, volume 3072 of *LNCS*, pages 1–7. Springer Verlag, 2004.

[10] Y. Matsuda, N. Miura, A. Nagasaka, H. Kiyomiu, and T. Miyatake. Finger-vein authentication based on deformation-tolerant feature-point matching. *Machine Vision and Applications*, 27(2):237–250, 2016.

[11] N. Miura, A. Nagasaka, and T. Miyatake. Feature extraction of finger-vein patterns based on repeated line tracking and its application to personal identification. *Machine Vision and Applications*, 15(4):194–203, 2004.

[12] N. Miura, A. Nagasaka, and T. Miyatake. Extraction of finger-vein patterns using maximum curvature points in image profiles. *IEICE transactions on information and systems*, 90(8):1185–1194, 2007.

[13] B. Prommegger, C. Kauba, and A. Uhl. Longitudinal finger rotation - problems and effects in finger-vein recognition. In *Proceedings of the International Conference of the Biometrics Special Interest Group (BIOSIG'18)*, Darmstadt, Germany, 2018.

[14] B. Ton and R. Veldhuis. A high quality finger vascular pattern dataset collected using a custom designed capturing device. In *International Conference on Biometrics, ICB 2013*. IEEE, 2013.

[15] L. Yang, G. Yang, Y. Yin, and X. Xi. Finger vein recognition with anatomy structure analysis. *IEEE Transactions on Circuits and Systems for Video Technology*, 2017.

[16] Y. Yin, L. Liu, and X. Sun. Sdumla-hmt: a multimodal biometric database. *Biometric Recognition*, pages 260–268, 2011.

[17] J. Zhang and J. Yang. Finger-vein image enhancement based on combination of gray-level grouping and circular gabor filter. In *Information Engineering and Computer Science, 2009. ICIECS 2009. International Conference on*, pages 1–4. IEEE, 2009.

[18] J. Zhao, H. Tian, W. Xu, and X. Li. A new approach to hand vein image enhancement. In *Intelligent Computation Technology and Automation, 2009. ICICTA'09. Second International Conference on*, volume 1, pages 499–501. IEEE, 2009.

[19] K. Zuiderveld. Contrast limited adaptive histogram equalization. In P. S. Heckbert, editor, *Graphics Gems IV*, pages 474–485. Morgan Kaufmann, 1994.